Tetrahedron 69 (2013) 10752–10762

Contents lists available at ScienceDirect

Tetrahedron

journal homepage: www.elsevier.com/locate/tet

Combined use of three forms of chiroptical spectroscopies in the study of the absolute configuration and conformational properties of 3-phenylcyclopentanone, 3-phenylcyclohexanone, and 3-phenylcycloheptanone

Patrizia Scafato [a], Francesca Caprioli [a,†], Laura Pisani [a], Daniele Padula [b], Fabrizio Santoro [c], Giuseppe Mazzeo [d], Sergio Abbate [d,*], France Lebon [d], Giovanna Longhi [d]

[a] Dipartimento di Scienze, Università della Basilicata, Via dell'Ateneo Lucano, 85100 Potenza, Italy
[b] Institute of Organic Chemistry and Biochemistry, Academy of Sciences, Flemingovo náměstí 2, 16610 Prague, Czech Republic
[c] CNR, Consiglio Nazionale delle Ricerche, Istituto di Chimica dei Composti Organometallici (ICCOM-CNR), UOS di Pisa, Area della Ricerca, via G. Moruzzi 1, 56124 Pisa, Italy
[d] Dipartimento di Medicina Molecolare e Traslazionale, Università di Brescia, Viale Europa 11, 25123 Brescia, Italy

ARTICLE INFO

Article history:
Received 26 July 2013
Received in revised form 23 September 2013
Accepted 7 October 2013
Available online 21 October 2013

We dedicate this work to the memory of Carlo Rosini, who suggested undertaking this study before his premature death

Keywords:
ORD
ECD
VCD
Vibronic features
Absolute configuration
Conformations
Phenyl hindered rotation

ABSTRACT

Three forms of chiroptical spectroscopies, electronic circular dichroism (ECD), vibrational circular dichroism (VCD), and optical rotatory dispersion (ORD) have been employed to study the configuration and conformational properties of the three molecules: (*S*)-3-phenylcyclopentanone, (*S*)-3-phenylcyclohexanone, and (*S*)-3-phenylcycloheptanone (including (*S*)-3-phenylcyclopentanone-2,2,5,5-d_4 and (*S*)-3-phenylcyclohexanone-2,2,6,6-d_4). ECD and VCD spectra in the mid-IR for the three molecular systems are marginally dependent on fine conformational details, as interpreted in terms of standard DFT computational methods, with common spectroscopic features to the three systems clearly identified. Accounting for vibronic coupling mechanisms reproduces the structuring of ECD $n \rightarrow \pi^*$ band. The ORD curves are quite similar for the three types of molecules, but their interpretation highlights a crucial role played by conformations of the cycloalkanone ring in the case of (*S*)-3-phenylcycloheptanone. The same conclusions are reached by considering the VCD spectra in the CH-stretching region.

1. Introduction

In the last 15–20 years, the increased availability of quantum-mechanical and computational methods, coded in easy-to-use and largely available packages, has enabled more and more scientists to better understand chiral molecules by predicting and comparing several experimental properties with computational analyses, disclosing new opportunities in the research field of chirality. Through the investigation of chiroptical properties,[1] like optical rotation (OR), optical rotatory dispersion (ORD), electronic circular dichroism (ECD) and vibrational circular dichroism (VCD),[2] it is possible nowadays to perform accurate structural analyses and to arrive at the safe determination of the molecular absolute configuration (AC). In many studies, chiroptical data of molecules having either known or unknown AC were correctly predicted. More recently the absolute configuration has been assigned mainly by the concerted use of these techniques.[3] The combined use of all these powerful chiroptical tools allows the AC determination of organic molecules to receive a safer solution. However, in spite of such significant progress, some relevant problems still remain: in particular, the treatment of molecules endowed with high conformational flexibility requires accurate calculation of the relative

* Corresponding author. E-mail address: abbate@med.unibs.it (S. Abbate).
† Present address: Stratingh Institute for Chemistry, Faculty of Mathematics and Natural Sciences, University of Groningen, Nijenborgh 4, 9747AG Groningen, The Netherlands.

0040-4020/$ – see front matter © 2013 Elsevier Ltd. All rights reserved.
http://dx.doi.org/10.1016/j.tet.2013.10.016

population and chiroptical response for each conformer in order to obtain the weighted average over the conformer populations of each property.

As pointed out above, the use of different chiroptical methods enables one to get an unambiguous and consistent description of the important structural and electronic molecular features. Since the conformational aspect may influence quite differently the various chiroptical data, on one hand one needs to pay attention in order to obtain an unequivocal response from all kinds of spectroscopies, on the other hand, a satisfactory matching between experiments and theory gives more information than the simple AC assignment. The systems herein studied are quite simple and for this reason they are a good benchmark to test computation potentiality. As we will show in this paper, despite improvements of theory and computation in the last years, the most primitive among chiroptical data, namely OR data still remain the most difficult ones to calculate.[4] We compare experimental and computational results from three techniques (ORD, ECD, and VCD) on three related model molecular systems, namely 3-phenylcycloalkanones **1**–**3** (Chart 1) synthesized by catalytic asymmetric addition of phenylboronic acid to the corresponding cycloalkenones.[5]

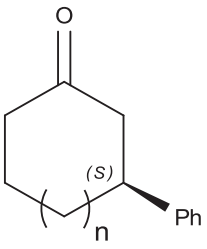

n = 0 (**1**)
n = 1 (**2**)
n = 2 (**3**)

Chart 1. Structures of studied compounds **1**–**3**.

2. Materials and methods

2.1. Synthesis and purification

3-Phenylcycloalkanones **1**–**3** were synthesized in 94–96% ee, as reported in Ref. 5a, by catalytic asymmetric addition of phenylboronic acid using (*S*)-BINAP/rhodium(I) complex, in the case of 3-phenylcyclopentanone 1,[5b] or a *tropos* phosphoramidite/rhodium(I) complex for cycloalkanones **2** and **3**.[5a] 3-Phenylcycloalkanones-d_4 **1′** and **2′** were prepared in 94% isotopic purity by refluxing the corresponding ketones in deuterium oxide, in presence of potassium carbonate (0.11 equiv), and monitoring the conversions by GC–MS analyses (see SI-part 1 for a detailed description of the experimental procedure and characterization of deuterated compounds). ^{1}H (400 MHz) NMR spectra were recorded in $CDCl_3$ on a Varian 400 NMR spectrometer, using tetramethylsilane (TMS) as internal standard. GC–MS analyses were performed on a Hewlett Packard 6890 gas chromatograph equipped with an HP-5973 mass detector and an HP-5MS capillary column.

2.2. ORD, ECD, and VCD spectra acquisition

ORD spectra were recorded with Jasco DIP370 digital polarimeter at four different wavelengths (589, 546, 435, 405 nm) in hexane for **1** and **2** and in chloroform for **3** at concentration of 1 g/100 mL (0.063 M, 0.057 M, and 0.053 M, respectively). Experimental ECD spectra were obtained by a JASCO 815SE apparatus from 400 to 180 nm under the following experimental conditions: integration time 1 s, scan speed 100 nm/min, bandpass 1 nm, 20 accumulations. Compounds **1**–**3** were measured in hexane solutions in 0.1 mm pathlength quartz cuvette. Concentrations were 0.0048 M, 0.0036 M, and 0.0058 M for **1**, **2**, and **3**, respectively. IR and VCD spectra were collected on a JASCO FVS4000 FTIR equipped with a liquid N_2-cooled MCT detector, 2000 accumulations were averaged in the 900–1800 cm^{-1} region at 4 cm^{-1} resolution, respectively. The spectra were obtained in CCl_4 solutions, in 100 μm pathlength BaF_2 cells for **1**, **2**, and **3** for 0.42 M, 0.35 M, and 0.21 M solutions, respectively. The VCD spectra in the CH-stretching region (2000–3200 cm^{-1}) were obtained on the same solution contained in the same cells, using the same apparatus with an InSb detector and with 5000 accumulations with 8 cm^{-1} resolution.

2.3. Computational details

The preliminary conformational analysis was performed on (3*S*) **1**–**3** by using the Spartan02[6] package with the MMFF94s molecular mechanics (MM) force field adopting Monte Carlo (MC) and Systematic options as search method. Geometries within 10 kcal/mol energy window have been re-optimized by Density Functional Theory (DFT) adopting the B3LYP functional and the TZVP basis set using the Gaussian09 package.[7] All investigated (ground-electronic state) conformers are real minima, no imaginary vibrational frequencies were found. Free energies were calculated and used to determine the Boltzmann populations of the conformers at 298.15 K.

Calculations of ORD and ECD spectra were performed by the TD-DFT approach using the Coulomb-attenuated CAM-B3LYP functional[8] and aug-cc-pVDZ as basis set. Theoretical ORD, ECD, and VCD spectra were obtained as averages weighted on the Boltzmann populations (VCD spectra were calculated at the B3LYP/TZVP level, as done for the conformer determination). The theoretical absorption and VCD spectra were simulated with Lorentzian bands with 4 cm^{-1} half-width at half maximum (HWHM) for the mid-IR and 16 cm^{-1} for the CH-stretching region. To best compare with experimental spectra, the computed frequencies have been scaled by a factor 0.985 in the mid-IR, and 0.97 in the CH-stretching region. The purely electronic ECD spectra were obtained as the sum of Gaussian functions centered at the calculated wavelength of each transition with the band area equal to the calculated rotational strength of the transition and the half-width at half maximum (HWHM) equal to 0.2 eV and elaborated using SpecDis v1.53.[9]

Vibronic features of ECD and absorption UV spectra were obtained in Frank–Condon (FC) approximation. In the excited state (ES) two minima characterized by a pyramidal arrangement of the CCC=O moiety are found, and they interconvert through a planar transition state. A rigorous treatment of the effect of the ES double-minimum profile along the carbonyl C pyramidalization (γ) would be challenging and require the following steps: (i) representation of the normal modes in internal coordinates; (ii) separation (if possible) of γ from the bath of the other harmonic modes, (iii) calculation of the anharmonic states supported by the ES energy profile along γ. Such an accurate simulation is beyond the scope of the present work, and here we resorted to a simpler approach, considering as ES reference geometry the transition state in which the CCC=O moiety is constrained to be planar, as it is at the ground-state (GS) equilibrium geometry. This strategy has been already adopted in similar cyclopentanone systems,[10,11] showing that it delivers results in reasonable agreement with experiment as far as the vibronic progressions along high-frequency modes are concerned; moreover, though the choice of the real frequency to be assigned to the pyramidalization mode is arbitrary (we simply considered the absolute value of the imaginary frequency), such

strategy is safer than trying to describe the ES vibronic states relevant for the spectrum, i.e., those whose population density covers the planar region, assuming that the ES PES is characterized by a single harmonic well centered at one of the two pyramidal geometries. As a matter of fact, simulations performed according to this later recipe, not reported, lead to completely structureless and extremely broad spectra. Vibronic calculations were performed by the FCClasses code,[12] in harmonic approximation,[13] employing the so-called Adiabatic Hessian approach (FC|AH). We adopted both an effective time-independent (TI) method based on a partition of the possible transitions into classes and on a prescreening technique for the individuation of the major stick bands[14] and a time-dependent (TD) method ensuring full convergence even at room temperature.[15] Convoluted spectra were obtained employing a Gaussian bandshape with HWHM=0.03 eV. Optimized geometries, normal modes and the corresponding frequencies of the electronic ground and excited states were obtained at DFT/B3LYP/TZVP level while the excitation energies and circular dichroism rotatory strengths were calculated at TDDFT/B3LYP/TVZP using Gaussian09.

3. Results and discussion

3.1. Conformational analysis

Preliminary MM based conformational analysis (with *S* AC on carbon 3) provided 4 low energy stable conformers for **1**, 5 for **2**, and 16 for **3**. The three sets of conformations lie within 10 kcal/mol and differ mostly by relative axial–equatorial phenyl position and by the cycloalkanone ring twist; phenyl hindered rotation and cycloalkanone ring twist interact as investigated in Supplementary data (Fig. SI-1) for (3*S*)-**3** for conformers **3a** and **3b** (vide infra), where the potential energy surface (PES) plots are given. Sets of conformations sorted by MM were then fully optimized at DFT/B3LYP/TZVP level of theory and provided the most likely conformers presented in Fig. 1. According to DFT results, basically compounds **1** and **2** exist in almost a single phenyl-equatorial conformation (more than 92% of the overall population). Higher flexibility of the seven-membered ring in **3**, resulted in eight DFT optimized conformers with a relative energy value less than 3 kcal/mol with respect to the most stable phenyl-equatorial conformer **3a**. Contrary to what happens in **1** and **2**, axial conformations of **3** do not appreciably contribute to overall population (the first most populated axial structure has 0.3% population, being 3.12 kcal/mol above the most stable conformer).

Cyclopentanone ring has a half-chair M-twisted conformation, cyclohexanone assumes the stable chair conformation and cycloheptanone is in a twisted pseudo-chair conformation (see Ref. 16, pp 174–181). Using the nomenclature introduced in Ref. 16 for (*R*)-3-methylcycloheptanone, in the case of molecule **3**, conformer **3a** is described as $TC_{7(-)}$ and conformer **3b** as $TC_{2(-)}$; no other conformer with appreciable population factor has been found. Phenyl moiety is in eclipsed conformation with respect to the hydrogen on stereogenic carbon 3.

We only considered as input geometries for chiroptical properties calculations the conformations with relative energies below 2 kcal/mol depicted in Fig. 1. Unlike **1** and **2**, the second populated conformer for **3** has a population factor comparable to the first one, being 0.85 of that.

3.2. Analysis of ORD data

Experimental ORD curves of **1**–**3** are very similar in sign, trend, and approximate magnitude of OR values measured at four different wavelengths (589, 546, 435, and 405 nm). Theoretical predictions failed somewhat to follow such simple similarity. A TDDFT/CAM-B3LYP/aug-cc-pVDZ level of theory was used in ORD prediction. In Fig. 2 we show comparison of experimental and calculated curves for **1**–**3**.

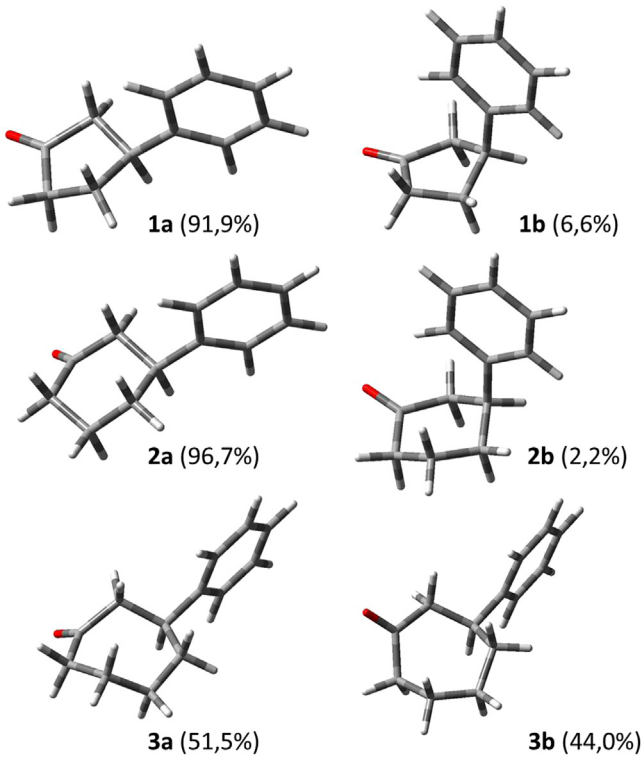

Fig. 1. Most stable conformers for molecules **1**–**3** as calculated at DFT/B3LYP/TZVP level of theory; **1a** (91.9%), and **1b** (6.6%), **2a** (96.7%), and **2b** (2.2%), **3a** (51.5%), **3b** (44.0%). Fixed AC is (3*S*)-**1**–**3**.

As shown in Fig. 2, TDDFT calculations predict experimental ORD curves of **1** and **2** in trend, sign, and magnitude (the latter characteristic is somewhat overestimated though). The case of **3** requires more attention. TDDFT ORD prediction at this level of theory, is not a 100% satisfactory even if the negative curve trend is accounted for. Calculated ORD is approximately five times smaller than the experimental (Table SI-1). This is indeed unexpected, in view of the very good consistency between experimental and calculated curves for **1** and **2** (we also notice that (*R*)-3-methylcycloheptanone gave an approximately enantiomeric ORD with respect to that of **3**[16,17]). Since the experimental ORD curves are similar for the three compounds and their absolute values have the same order of magnitude, we considered a few possible sources of errors for compound **3**. As previously shown, compound **3** has two main conformers, both with the phenyl in equatorial conformation, similar in relative populations (51.5% for conformer **3a** and 44.0% for **3b**) but differing in cycloheptanone ring conformation (Fig. SI-2) (It is reassuring to learn that also for (*R*)-3-methylcycloheptanone, important conformer dependence of ECD spectra was observed.[16,18]). The conformation, which best fits experimental data is **3b**, for this reason we thought it was possible that the employed level of theory did not properly describe the two conformations relative energies. We thus increased basis sets level using (with B3LYP functional) aug-cc-pVDZ and cc-pVTZ. Use of different basis sets did not lead to significant changes (Table SI-2). Moreover use of aug-cc-pVDZ basis set promoted conformer **3a** to 62.1% (Fig. 3).

Also adoption of the IEF-PCM[19] solvent model in the optimizations (chloroform) at DFT/B3LYP/TZVP level reveals no significant change in the relative population of conformers (Table SI-2). We also performed ORD calculation with PCM model (chloroform) at

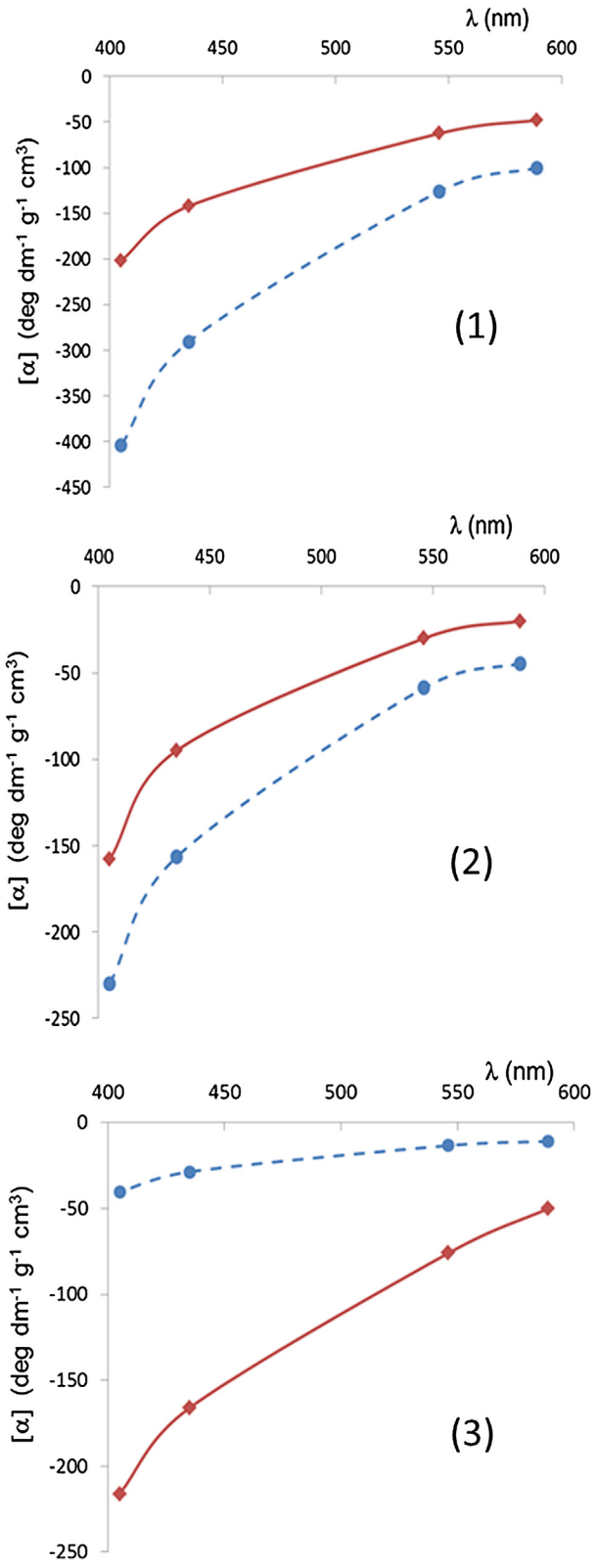

Fig. 2. Comparison of calculated (dashed blue lines, TDDFT/CAM-B3LYP/aug-cc-pVDZ on DFT/B3LYP/TZVP input geometries) and experimental (solid red lines, (1) and (2) hexane, (3) chloroform) ORD curves of **1**–**3**. Fixed AC are (3*S*)-**1**–**3**.

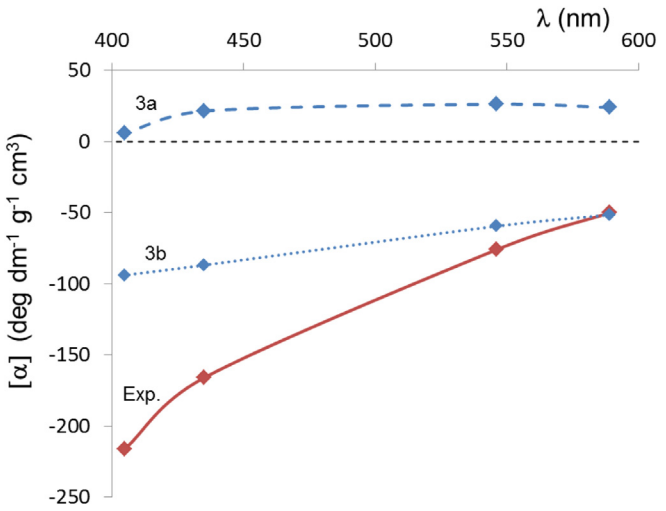

Fig. 3. Comparison of calculated (TDDFT/CAM-B3LYP/aug-cc-pVDZ on DFT/B3LYP/TZVP input geometries) ORD curves for **3a** (dashed blue line), **3b** (dotted blue line) and experimental (solid red line, chloroform).

TDDFT/CAM-B3LYP/aug-cc-pVDZ level (Table SI-3). The ORD curve of **3a** is still positive except for the $[\alpha]_{405}$ value, which turns out slightly negative (−3.56).

Another source of discrepancy between experimental and calculated ORD curves could be the quite flat energy dependence from the phenyl dihedral angle, which makes multiple orientations of the phenyl group thermally accessible. Then a correct prediction of ORD possibly requires those structures to be analyzed and computed in order to be considered in the averaged property. We performed a relaxed scan along the phenyl torsion C_9–C_8–C_3–H_3 (φ) for both **3a** and **3b** (at DFT/B3LYP/TZVP level), with a stepsize of 20° of dihedral angle (Fig. 4).

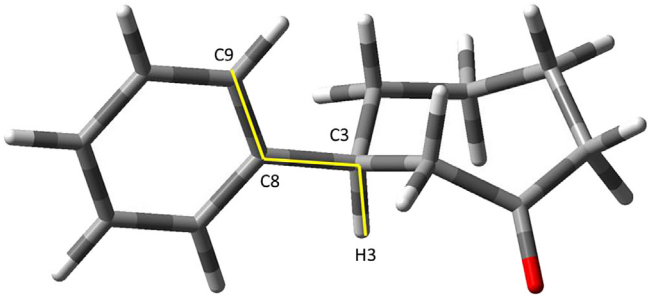

Fig. 4. Numbering of dihedral angle φ considered in performing optimizations scan of **1**–**3**.

In a section of Supplementary data dedicated to the analysis of ORD for (*S*)-3-phenylcycloheptanone, we have evaluated and compared the energy and ORD dependence on φ and compared results for **3a** and **3b** with those for **1** and **2** (Table SI-4, Figs. SI-3–5).

3.3. Analysis of ECD spectra

UV and ECD spectra were recorded in hexane and CCl_4. ECD spectra of **1**–**3** (Fig. 5) all show a negative and vibrationally resolved (vide infra) Cotton effect (CE) centered at 300 nm, which is ascribed to n–π^* carbonyl transition (this happens also for other substituted cycloalkanones[11,16]). The vibronic structure fades away with increasing ring dimensionality. Two positive CEs centered at 220 nm

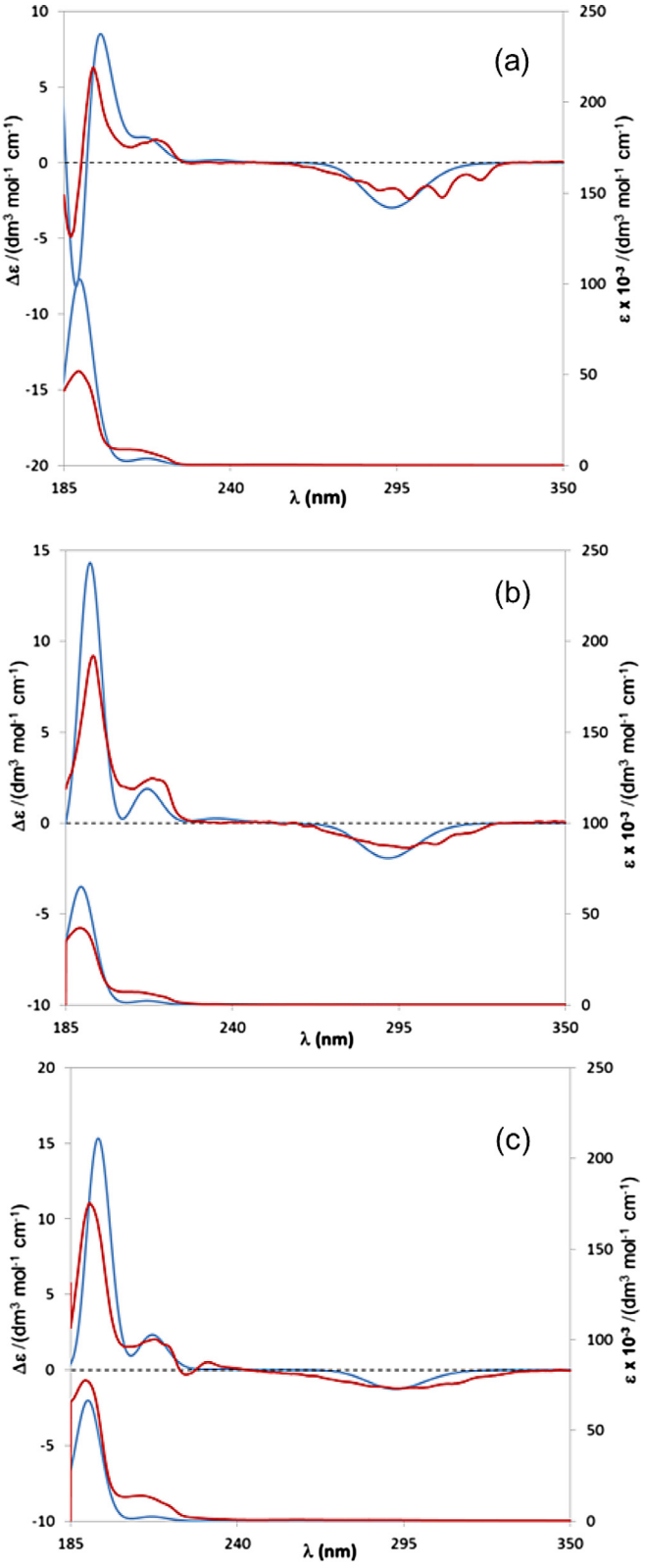

Fig. 5. Experimental ECD (top red lines, hexane), experimental UV (bottom red lines, hexane), and calculated ECD (top blue lines), UV (bottom blue lines) comparison spectra of **1** (plot a), **2** (plot b), and **3** (plot c). Calculated ECDs were performed at TDDFT/CAM-B3LYP/aug-cc-pVDZ (IEF-PCM, hexane) on DFT/B3LYP/TZVP input geometries, 30 first excited states, 0.2 eV of bandwidth. All calculated spectra are 5 nm red shifted, calculated UV and ECD of **1** have been divided by 2, those for **2** and **3** by 3 (see text).

and 196 nm (allied to ^1L_a and ^1B_b benzene transitions, respectively) are present for all three molecules. ECD spectrum of **3** shows an additional weak positive band at 230 nm ascribed to ^1L_b transition and a negative CE at about 186 nm is present in the ECD of **1**. These bands are allied to $\pi-\pi^*$ benzene transitions. ECD calculations were performed at TDDFT/CAM-B3LYP/aug-cc-pVDZ level of theory both in gas phase and according to a hexane IEF-PCM calculation, taking into account the first 30 excited states. Length and velocity formalisms led to similar rotational strengths prediction; then only velocity rotatory strengths based ECD shapes are displayed. Notwithstanding a quite good prediction based on gas phase calculations (Fig. SI-6) we report in Fig. 5 ECD calculations based on solvation model, allowing to better predict in magnitude the experimental spectra in the 190–200 nm range. Equatorial conformations, of **1** and **2**, drive negative sign of the $n-\pi^*$ CE, which is consistent with the experimental ones and with the octant rule.[16] The two equatorial conformations **3a** and **3b** possess opposite $n-\pi^*$ sign and consistent with octant rule. Conformer **3a**, which is the most populated one, has a negative CE as in the experimental spectrum (vide infra). The existence of multiple conformers was postulated in Refs. 16–18 for (*R*)-3-methylcycloheptanone and was demonstrated by running temperature dependent ECD spectra, where better resolved vibronic features were evidenced at lower temperatures.[18] Calculations also exhibit weak positive CE associated with ^1L_b transition at 240 nm, which are not easily visible in **1** and **2** experimental spectra. On the other hand positive CE of **3**, related to ^1L_b transition, is predicted even if, due to the Boltzmann averaging, its rotatory strength is very weak (+0.17). It is important to note that the nice matching between calculated and experimental UV profiles leads to reliable and safe assignment of corresponding ECD bands. Comparison of theoretical and experimental ECD spectra of **1**–**3** shows good agreement with a full prediction of experimental CEs in sign, position and intensities (Fig. 5).

On the side of ECD calculation it is important to note that conformers **3a** and **3b** have again an enantiomeric behavior (Fig. 6) and the most populated conformer **3a** is the one with the correct ECD signs (cf. the results for (*R*)-3-methylcycloheptanone[18]) but the correct intensity is obtained only considering both conformers.

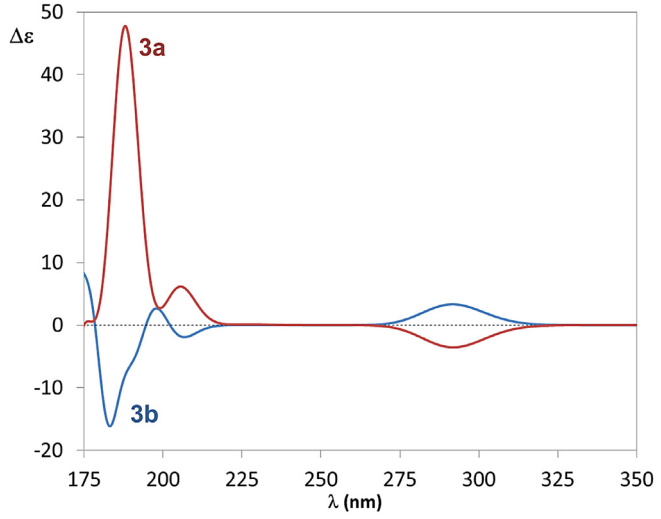

Fig. 6. Calculated ECD spectra comparison for conformers **3a** (solid red line) and **3b** (solid blue line) at TDDFT/CAM-B3LYP/aug-cc-pVDZ-(IEF-PCM, hexane) level, on DFT/B3LYP/TZVP-(IEF-PCM, hexane) calculated geometries, 30 first excited states, 0.2 eV bandwidth.

In contrast to the ORD case, the results of ECD calculations are off with respect to experiment by a smaller factor except for **3**, since

the ECD spectrum is due to cancellation of two oppositely signed ECD spectra for conformers **3a** and **3b** and the ECD spectrum of the more populated conformer **3a** better matches the experimental data. We checked that phenyl rotation of $+/-10^{\circ}$ does not affect ECD calculation confidence, despite a difference in relative intensities of rotatory strengths for the bands below 190 nm while the effect on ORD for the same changes is quite dramatic (Fig. SI-7).

The vibronic structure of n–π^* ECD bands in (*R*)-3-methylcycloalkanones were discussed at length in Refs. 16 and 18. In Fig. 7 we compare to experiment the calculated vibronically resolved bands for **1**–**3** allied to the n–π^* low lying transition (we considered only equatorial conformations of **1**, **2**, and **3** and, for the latter systems, both **3a** and **3b** species). Before presenting the results, it should be emphasized that the ECD spectra of **1**, **2**, and **3** compounds mainly differ in width and resolution, and that the specific properties of the manifold of the anharmonic states along the CCC=O pyramidalization, here neglected, would probably have an impact on such spectral features. With this limitation in mind, we can notice that the results obtained with harmonic approximation still match a number of experimental findings. Let us focus on the spectra computed at 300 K. In agreement with experiment, the spectra of the three species show a characteristic progression, observed in experiments, that is due to the CO stretching. Two additional features agree with experiment: (i) moving from **1** to **2** and **3** the peaks of the CO vibronic progression are less and less 'resolved', finally reducing to a weak modulation of a broad and unstructured background in **3a**/**3b**; (ii) the maxima of the **3a** and **3b** spectra are blueshifted with respect to those of **1** and **2**. The former phenomenon (i) is, at least partially, due to the fact that the normal

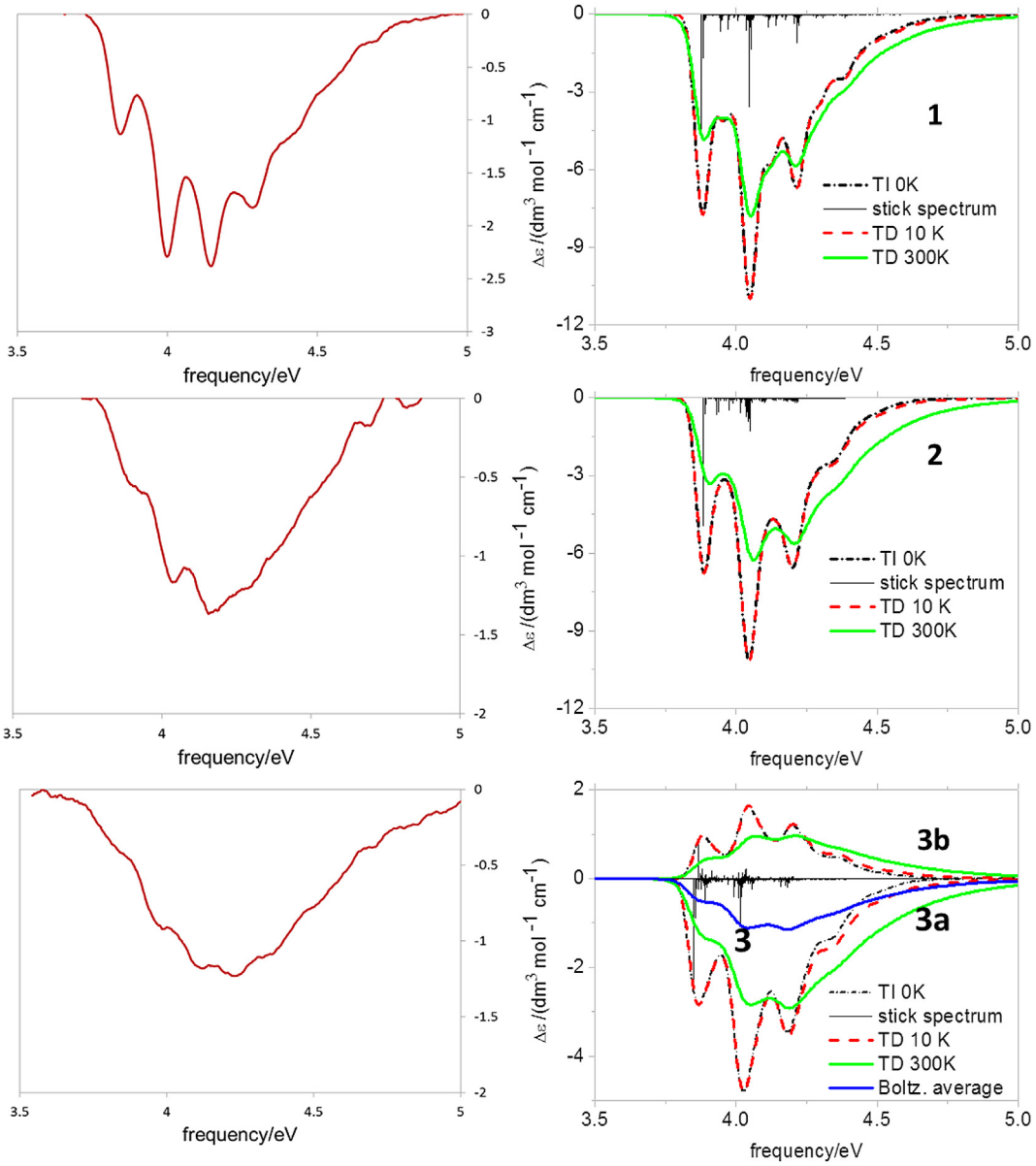

Fig. 7. Comparison of experimental (left panels) and theoretical (right panels) absorption UV spectra of n–π^* electronic transition of **1**, **2** and **3** in a range from 3.5 to 5 eV calculated within FC|AH approximation (see text).

modes that are related to the CO stretching exhibit an increased Duschinsky mixing moving from **1** to **3**, so that while a single dominant progression is seen in **1**, a larger number of (weaker) vibronic transitions, with close but different energies, contribute to the **3a**/**3b** ECD lineshape. The same mechanism explains also the

blueshift of the **3a**/**3b** maxima, but in this case also thermal excitation plays an essential role and in fact the blueshift is not observed at 10 K. The existence of two conformers of comparable population represents an additional factor leading to a blurring of the **3** spectrum. This is shown in the bottom panel of Fig. 7 comparing the ECD spectra of the **3a** and **3b** with their Boltzmann average (notice however that the computed Boltzmann populations cannot be considered free of errors).

3.4. Analysis of VCD spectra

Experimental vibrational absorption (VA) and VCD spectra, measured in CCl_4 solutions were analyzed and compared with calculated ones at DFT/B3LYP/TZVP level of theory considering (3*S*)-**1**–**3** as fixed AC. In Figs. 8–10 we compare experimental and predicted (for each most stable conformation and Boltzmann average) VA and VCD spectra in the mid-IR region (900–1600 cm^{-1}). As configurational assignment. Accordingly DFT calculations, which provide good simulation of these bands in sign and magnitude, allow to attribute the negative feature to phenyl C–H in-plane bendings coupled to C*–H in-plane bending, whilst the positive counterpart is associated to CH_2 bending mode of units 4 for **1** and units 4 and 5 for **2** in the cycloalkanone ring, coupled to little C*–H bending. This feature is also present in the deuterated d_4 (Chart 2) derivatives (**1′** and **2′**) of **1** and **2**, which possess the same vibrational normal modes of their non-deuterated counterparts (In Fig. 8 we show that both VA and VCD calculated spectra for **1′** compare also favorably with experiments.).

Proceeding with the analysis of VA/VCD spectra of **1**, we notice that the intense band numbered as 33 in the VA spectrum in Fig. 8 is calculated at slightly different frequencies for the two conformers, close to the weak features #34 and 35 and corresponds to the multiple bands group in the experimental spectrum (from here on we speak of band # and normal mode # interchangeably, when no

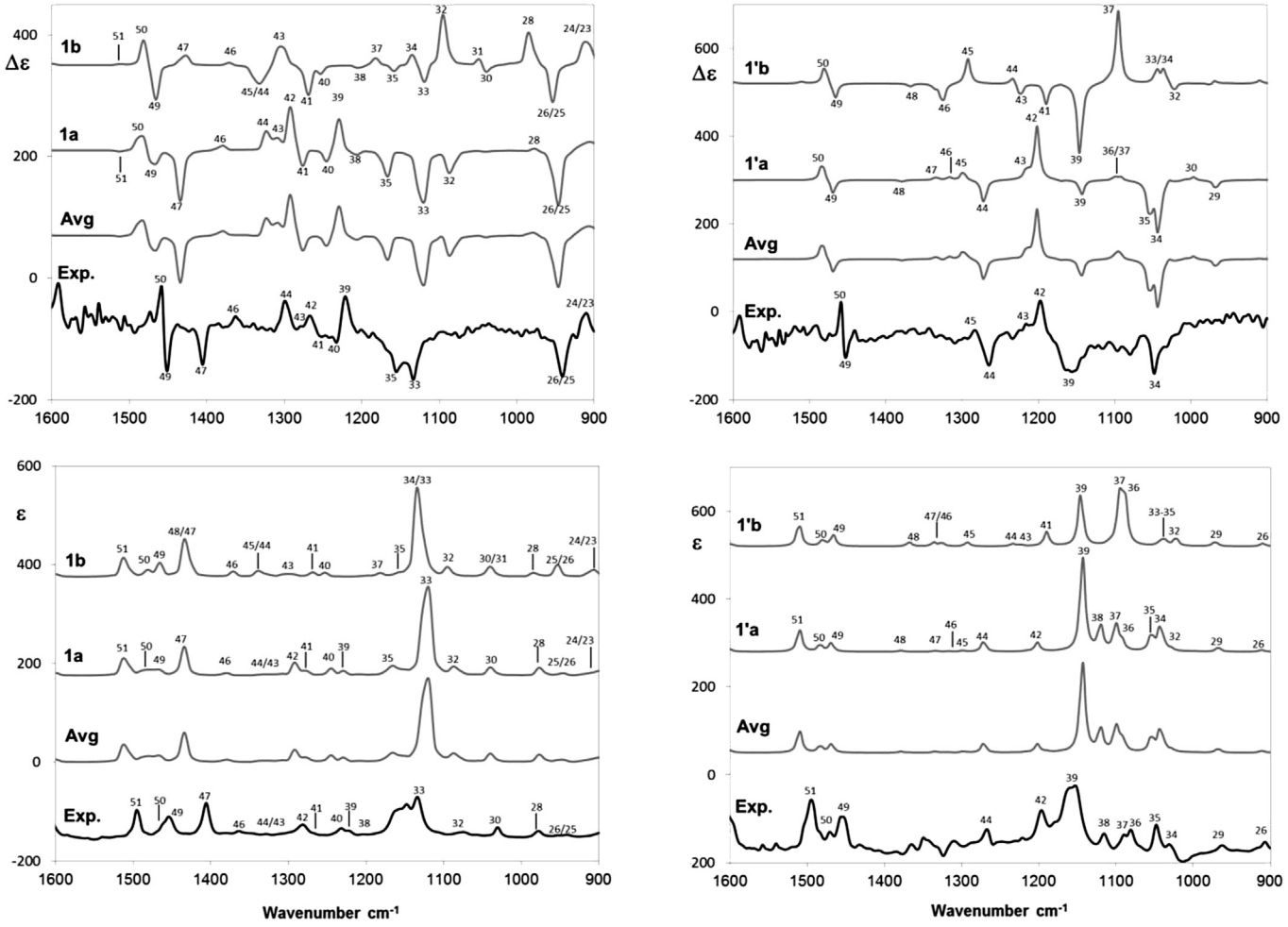

Fig. 8. Comparison of experimental and calculated VA (bottom panels) and VCD (top panels) spectra for **1** and deuterated **1′** (see Chart 2). Experimental spectra (exp. traces) are measured in CCl_4. Calculated spectra of equatorial conformations **1a** and **1′a** (deuterated equatorial conformer), axial conformations **1b** and **1′b** (deuterated axial conformer) and Boltzmann's averaged spectra (avg traces) are computed at DFT/B3LYP/TZVP level.

a general qualitative comparison there is a clear matching between experimental and calculated spectra, which are mainly determined by the major conformer. In particular, we observe that a bisignate negative–positive feature at 1450–1457 cm^{-1} for **1**, **2** and 1440–1453 cm^{-1} for **3** appears in the VCD spectra, including the deuterated counterparts of **1** and **2**: for this reason we think that this couplet has the characteristics of a marker signal for confusion is caused, i.e., when one conformer is prevalent). According to DFT calculation, the normal modes associated to band #33 are mainly the C–C in-plane anti-symmetric stretching of the CC bond pair in the alkanone ring sharing the carbonyl carbon atom. The modes are also coupled to some in-plane benzene group C–H bendings. It is interesting to note that bands 28 and 32, which are present in the VCD of the axial conformer **1b**, do not appear in

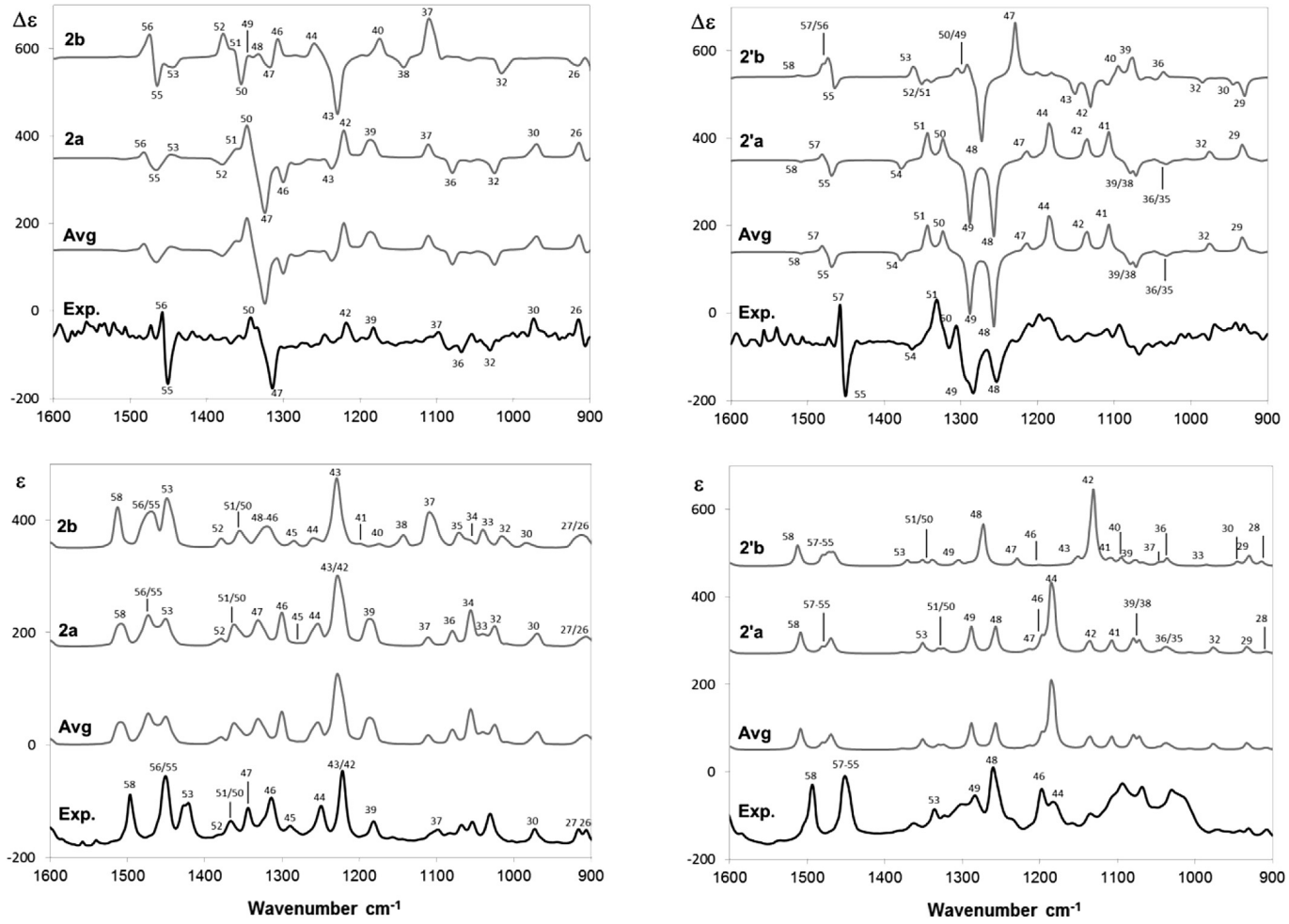

Fig. 9. Comparison of experimental and calculated VA (bottom panels) and VCD (top panels) spectra for **2** and deuterated **2′** (see Chart 2). Experimental spectra (exp. traces) are measured in CCl_4. Calculated spectra of equatorial conformations **2a** and **2'a** (deuterated equatorial conformer), axial conformations **2b** and **2'b** (deuterated axial conformer) and Boltzmann's averaged spectra (avg traces) are computed at DFT/B3LYP/TZVP level.

the measured spectrum, confirming low experimental contribution of axial conformation but with not as sufficient finesse as previously done by He et al.,[20] where (*R*)-3-methylcyclopentanone was investigated and the relative ratio of axial and equatorial conformers was determined.

In Fig. 9 comparison of experimental and calculated VA and VCD spectra of **2** and **2′** is reported.

Main VA and VCD experimental features are well predicted. The predicted VCD intense negative band 43 at 1230 cm^{-1} for the axial conformation (related to some CH_2 wagging on the cyclohexanone ring) does not appear in experimental spectrum, confirming too low contribution of axial conformation to be detected, within the limits of the quality of our experiments. Possibly also normal modes # 47 (+VCD) and # 48 (−VCD) of the axial conformer of the d_4 homologue manifest themselves in the experimental VCD spectra. However these conclusions are only qualitative: we notice that in the analogous case of (*R*)-3-methyl cyclohexanone, the use of mid-IR VCD allowed to quantitatively define the relative content of axial versus equatorial conformation. In this case we have a lower contribution of axial conformer than the one at 10% as found by Devlin and Stephens.[21]

The VA spectrum of **3** in the 900–1300 cm^{-1} region (Fig. 10) presents weak signals. Anyway in correspondence of experimental bands at ca. 1150 and 1200 cm^{-1} it is possible to find in the calculated average spectrum the couples of bands 41 and 42, belonging to **3a** and **3b**, respectively, and 44–46, for **3a** and **3b**, respectively. The corresponding experimental VCD spectrum shows very weak features in that range. At higher wavenumbers, the calculated average VCD spectrum shows a bisignate couplet (at ca. 1350 cm^{-1}) arising from modes 54 and 56 almost exclusively from conformer **3a**. The normal modes involved are due to C*–H bending and CH_2 twistings in methylene units of the cycloheptanone ring. Even if very weak, in the experimental VCD spectrum, we note a non-conservative bisignate couplet at 1250 cm^{-1} ascribed to CH_2 twistings. The positive band, referred to mode 48 results from **3a** conformation whilst weaker negative 47 band is from conformer **3b**. Negative CE numbered 30 (rock CH_2 bendings and cycloheptanone ring deformation) is also well predicted. We have checked the sensitivity of the VCD technique to phenyl moiety rotation of **3** by considering structures **3**α and **3**β. In Fig. SI-8 a comparison of experimental VA and VCD spectra with the calculated spectra for separate conformations **3a**, **3**α and **3**β and their Boltzmann average is presented. Both **3**α and **3**β VA spectra appear quite similar but broadening of band group 38–40 manifests in **3**β, which relates to a C–C stretching affecting the stereogenic carbon atom. In the VCD trace of **3**β a positive band 41 allied to C*–H bending creeps in. It appears that vibrational local modes affecting the chiral carbon atom may somewhat change VCD response. Anyway the overall matching with the VA and VCD data for most stable **3a** is acceptable.

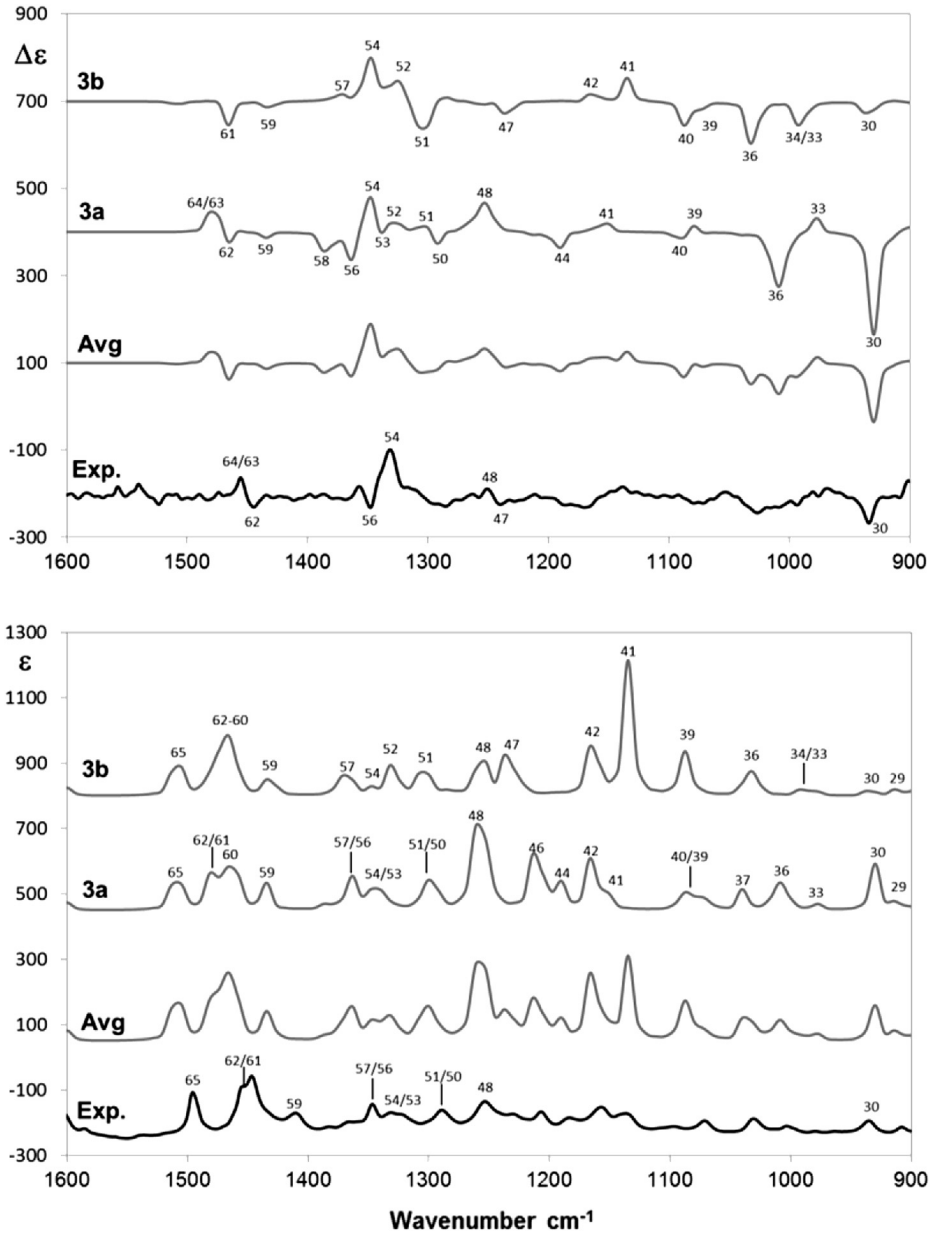

Fig. 10. Comparison of experimental and calculated VA (bottom panel) and VCD (top panel) spectra for **3**. Experimental spectra (exp. traces) are measured in CCl_4. Calculated spectra of equatorial conformations **3a** and **3b** and Boltzmann's averaged spectra (avg traces) are computed at DFT/B3LYP/TZVP level.

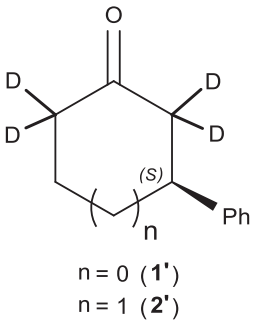

n = 0 (**1'**)
n = 1 (**2'**)

Chart 2. Structures of deuterated homologues of compounds **1** and **2**.

Finally we investigated the C–H stretching fundamental region (2800–3100 cm^{-1}), a region, which has been recently overlooked, even though it was the focus of the first VCD investigations.[22,23] In Figs. 11–13 comparison of calculated and experimental spectra for (*S*)-**1**, **2**, and **3**, respectively, is reported. VCD features in the range of 2900–3000 cm^{-1} are generated by cycloalkanones methylene C–H stretchings. In compound **1** (Fig. 11), according to DFT/B3LYP/TZVP calculation, the experimental VCD positive feature at 2900 cm^{-1} arises from C–H stretching of axial hydrogen in C5 position of **1a**.

The negative experimental CE at 2970 cm^{-1} corresponds to the negative band of conformer **1a** related to symmetric stretchings of axial hydrogen at C4 and equatorial hydrogen at C5. Axial conformer **1b** provides enantiomeric VCD behavior to equatorial conformer **1a**, and this had been recognized some time ago on a semi-empirical basis:[24,25] since the experimental VCD spectrum is justified by **1a** data, we have another proof of the minor importance of the axial conformer.

Also in the case of **2** (Fig. 12) the experimental VCD spectrum reveals a (−,+,−) structure between 2900 and 2970 cm^{-1}, which

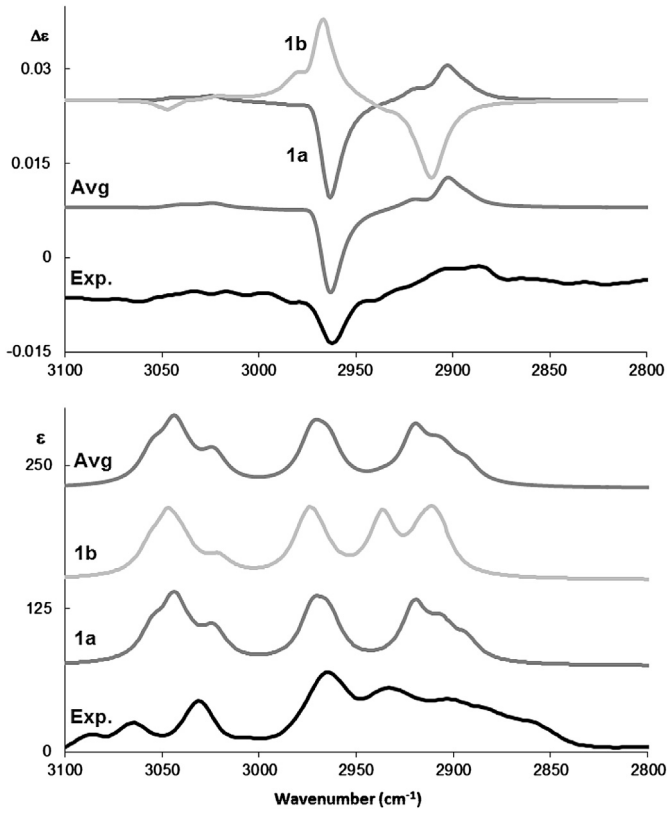

Fig. 11. Comparison of experimental and calculated VA (bottom panel) and VCD (top panel) spectra for **1** in the C–H stretching region (2800–3100 cm^{-1}). Experimental spectra (exp. traces) are measured in CCl_4. Calculated spectra of equatorial and axial conformations **1a** and **1b** respectively and Boltzmann's averaged spectra (avg traces) are computed at DFT/B3LYP/TZVP level.

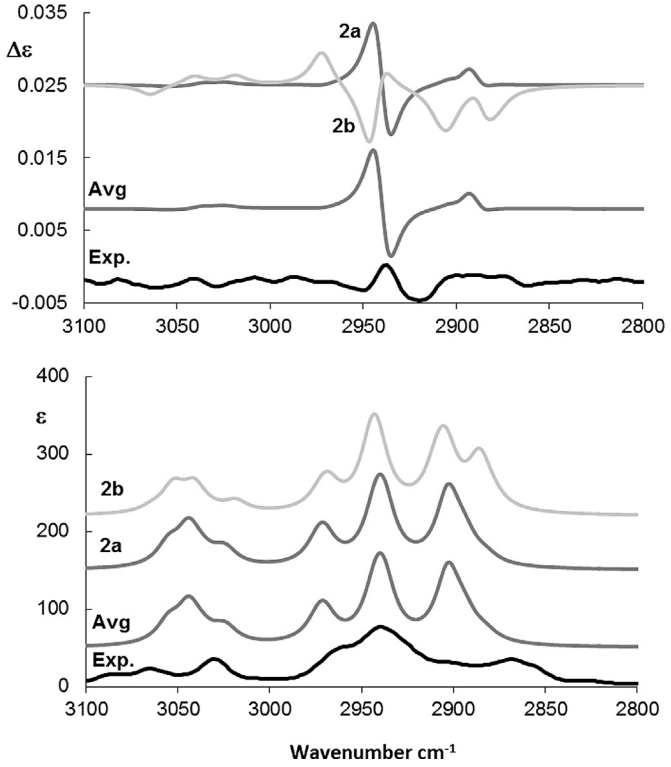

Fig. 12. Comparison of experimental and calculated VA (bottom panel) and VCD (top panel) spectra for **2** in the C–H stretching region (2800–3100 cm^{-1}). Experimental spectra (exp. traces) are measured in CCl_4. Calculated spectra of equatorial and axial conformations **2a** and **2b** respectively and Boltzmann's averaged spectra (avg traces) are computed at DFT/B3LYP/TZVP level.

has been known for 30 years for (*R*)-3-methylcyclohexanone[24] (as opposite) and attributed to concerted normal modes involving the stretching of C*–H and the anti-symmetric stretchings of the two CH_2 units 4 and 5 near the stereogenic carbon atom. Later this situation was further studied and called as vibrational excitons.[25] The three units are mirror images of each other in axial (**2b**) and equatorial (**2a**) conformers and this justifies the calculated VCD spectra being opposite. Correspondence of experimental and calculated VCD for **2a** rules out the presence of **2b** (as already obtained by mid-IR VCD, ECD, and ORD).

In the case of **3** ((*S*)-3-phenylcycloheptanone) (Fig. 13) the VCD behavior in this region for **3a** and **3b** is enantiomeric. Since the population factors of **3a** and **3b** are similar, this leads to almost a cancellation of the two VCD traces. However **3a** is slightly more populated than **3b** and this allows to predict right signs for the VCD spectrum; and also justifies why one does not observe the usual spectrum with alternating signs.[24,25] Together with ORD, VCD in the CH-stretching region provides the most compelling evidence of the conformational equilibria in the cycloheptanone ring. Further data on d_4-isotopomers in the CD stretching region for **1** and **2** are presented in Supplementary data.

4. Conclusions

In the present work we have investigated the configuration and conformational properties of (*S*)-3-phenylcyclopentanone (**1**), (*S*)-3-phenylcyclohexanone (**2**), and (*S*)-3-phenylcycloheptanone (**3**) and some deuterated species thereof. Indeed we have noticed that, notwithstanding the copious literature on the synthesis of these compounds, no complete analysis, based on advanced chiroptical

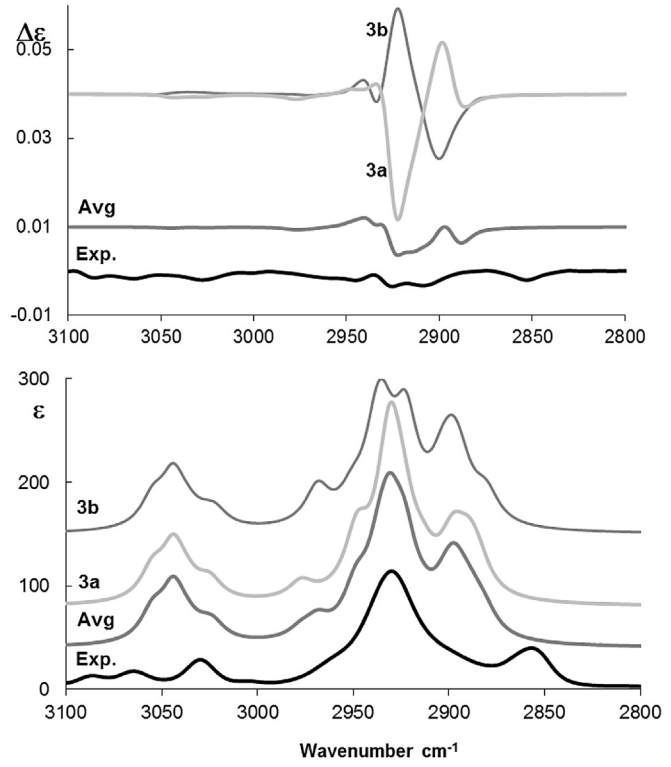

Fig. 13. Comparison of experimental and calculated VA (bottom panel) and VCD (top panel) spectra for **3** in the C–H stretching region (2800–3100 cm^{-1}). Experimental spectra (exp. traces) are measured in CCl_4. Calculated spectra of equatorial conformations **3a** and **3b** and Boltzmann's averaged spectra (avg traces) are computed at DFT/B3LYP/TZVP level.

and conformational studies, exists.[26] All chiroptical data for **1**, **2**, and **3**, with one exception, look similar, namely experimental ECD spectra are almost identical for **1**, **2**, and **3**; experimental VCD and VA spectra in the mid-IR for **1**, **2**, and **3** show common features and ORD curves are quite similar for **1**, **2**, and **3**; only in the CH-stretching region the VCD data for **3** look special. From this we conclude that the configuration is the same for the three molecules, however the conformational properties are similar, though not identical, as predicted at DFT level and confirmed by good comparison with experiments. Indeed the ECD and VCD spectra are correctly interpreted by DFT calculations in terms of a prevalent percentage of the equatorial conformer of the phenyl moiety with the ring being half-chair for **1**, stable chair for **2**, and twisted pseudo-chair conformers for **3**. However, while in the former two cases the prevalent conformer has a major importance being about 95% of the total, in the last case there is a second conformer with inferior but similar statistical weight and opposite chiroptical properties. The ORD and VCD data in the CH-stretching region are the most sensitive to these conformational details.

Acknowledgements

G.M. and G.L. wish to thank Cariplo Foundation, Milan, Italy, for funding a post-doc position. F.S. acknowledges support from MIUR (PRIN 2010–2011 prot. 2010ERFKXL).

Supplementary data

Supplementary data associated with this article can be found in the online version, at http://dx.doi.org/10.1016/j.tet.2013.10.016.

References and notes

1. The general theory of optical activity is given by (a) Rosenfeld, L. *Z. Phys.* **1928**, *52*, 161–171; (b) Condon, E. U. *Rev. Mod. Phys.* **1937**, *9*, 432–457; (c) Buckingham, A. D. *Adv. Chem. Phys.* **1967**, *12*, 107–142.
2. For general discussion of the ab initio calculation of chiroptical properties: (a) *Comprehensive Chiroptical Spectroscopy: Applications in Stereochemical Analysis of Synthetic Compounds, Natural Products, and Biomolecules*; Berova, N., Polavarapu, P. L., Nakanishi, K., Woody, R. W., Eds.; John Wiley & Sons: Hoboken, NJ, USA, 2012; (b) Autschbach, J. *Chirality* **2009**, *21*, E116–E152; (c) Autschbach, J.; Nitsch-Velasquez, L.; Rudolph, M. *Top. Curr. Chem.* **2011**, *298*, 1–98; (d) Yang, G.; Xu, Y. *Top. Curr. Chem.* **2011**, *298*, 189–236.
3. (a) Stephens, P. J.; McCann, D. M.; Butkus, E.; Stoncius, S.; Cheeseman, J. R.; Frisch, M. J. *J. Org. Chem.* **2004**, *69*, 1948–1958; (b) Stephens, P. J.; McCann, D. M.; Devlin, F. J.; Cheeseman, J. R.; Frisch, M. J. *J. Am. Chem. Soc.* **2004**, *126*, 7514–7521; (c) Stephens, P. J.; McCann, D. M.; Devlin, F. J.; Flood, T. C.; Butkus, E.; Stoncius, S.; Cheeseman, J. R. *J. Org. Chem.* **2005**, *70*, 3903–3913; (d) Stephens, P. J.; McCann, D. M.; Devlin, F. J.; Smith, A. B., III. *J. Nat. Prod.* **2006**, *69*, 1055–1064; (e) Stephens, P. J.; Pan, J. J.; Devlin, F. J.; Krohn, K.; Kurtan, T. *J. Org. Chem.* **2007**, *72*, 3521–3536; (f) Stephens, P. J.; Pan, J. J.; Devlin, F. J.; Urbanova, M.; Hajicek, J. *J. Org. Chem.* **2007**, *72*, 2508–2524; (g) Polavarapu, P. L.; He, J.; Crassous, J.; Ruud, K. *ChemPhysChem* **2005**, *6*, 2535–2540; (h) Petrovic, A. G.; He, J.; Polavarapu, P. L.; Xiao, L. S.; Armstrong, D. W. *Org. Biomol. Chem.* **2005**, *3*, 1977–1981; (i) Petrovic, A. G.; Polavarapu, P. L.; Drabowicz, J.; Zhang, Y.; McConnell, O. J.; Duddeck, H. *Chem.—Eur. J.* **2005**, *11*, 4257–4262; (j) Zuber, R.; Goldsmith, M.; Hopkins, T. D.; Beratan, D.; Wipf, P. *Org. Lett.* **2005**, *23*, 5269–5272; (k) Zuber, R.; Goldsmith, M.; Beratan, D.; Wipf, P. *Chirality* **2005**, *17*, 507–510; (l) Marchesan, D.; Coriani, S.; Forzato, S.; Nitti, P.; Pitocco, G.; Ruud, K. *J. Phys. Chem. A* **2005**, *109*, 1449–1453; (m) Cheng, M.; Li, Q.; Lin, B.; Sha, Y.; Ren, J.; He, Y.; Wang, Q.; Hua, H.; Ruud, K. *Tetrahedron: Asymmetry.* **2006**, *17*, 179–183; (n) Voloshina, E.; Fleischhauer, J.; Kraft, P. *Helv. Chim. Acta* **2005**, *88*, 194–209; (o) Sebert, S.; Konig, G. M.; Voloshina, E.; Raabe, G.; Fleischhauer, J. *Chirality* **2006**, *18*, 413–418; (p) Mazzeo, G.; Santoro, E.; Andolfi, A.; Cimmino, A.; Troselj, P.; Petrovic, A. G.; Superchi, S.; Evidente, A.; Berova, N. *J. Nat. Prod.* **2013**, *76*, 588–599.
4. (a) Stephens, P. J.; Pan, J. J.; Devlin, F. J.; Cheeseman, J. R. *J. Nat. Prod.* **2008**, *71*, 285–288; (b) Mazzeo, G.; Giorgio, E.; Zanasi, R.; Berova, N.; Rosini, C. *J. Org. Chem.* **2010**, *75*, 4600–4603; (c) Mazzeo, G.; Giorgio, E.; Rosini, C.; Fabris, F.; Fregonese, E.; Toniolo, U.; Lucchi, O. D. *Chirality* **2009**, *21*, E86–E97.
5. (a) Scafato, P.; Caprioli, F.; Rosini, C. *Tetrahedron: Asymmetry* **2011**, *22*, 558–561; (b) Takaya, Y.; Ogasawara, M.; Hayashi, T.; Sakai, M.; Miyaura, N. *J. Am. Chem. Soc.* **1998**, *120*, 5579–5580.
6. SPARTAN 02. Wavefunction: Irvine, CA.
7. Frisch, M. J.; Trucks, G. W.; Schlegel, H. B.; Scuseria, G. E.; Robb, M. A.; Cheeseman, J. R.; Scalmani, G.; Barone, V.; Mennucci, B.; Petersson, G. A.; Nakatsuji, H.; Caricato, M.; Li, X.; Hratchian, H. P.; Izmaylov, A. F.; Bloino, J.; Zheng, G.; Sonnenberg, J. L.; Hada, M.; Ehara, M.; Toyota, K.; Fukuda, R.; Hasegawa, J.; Ishida, M.; Nakajima, T.; Honda, Y.; Kitao, O.; Nakai, H.; Vreven, T.; Montgomery, J. A., Jr.; Peralta, J. E.; Ogliaro, F.; Bearpark, M.; Heyd, J. J.; Brothers, E.; Kudin, K. N.; Staroverov, V. N.; Kobayashi, R.; Normand, J.; Raghavachari, K.; Rendell, A.; Burant, J. C.; Iyengar, S. S.; Tomasi, J.; Cossi, M.; Rega, N.; Millam, J. M.; Klene, M.; Knox, J. E.; Cross, J. B.; Bakken, V.; Adamo, C.; Jaramillo, J.; Gomperts, R.; Stratmann, R. E.; Yazyev, O.; Austin, A. J.; Cammi, R.; Pomelli, C.; Ochterski, J. W.; Martin, R. L.; Morokuma, K.; Zakrzewski, V. G.; Voth, G. A.; Salvador, P.; Dannenberg, J. J.; Dapprich, S.; Daniels, A. D.; Farkas, Ö.; Foresman, J. B.; Ortiz, J. V.; Cioslowski, J.; Fox, D. J. *Gaussian 09, Revision A.02*; Gaussian, Inc.: Wallingford, CT, 2009.
8. (a) Yanai, Y.; Tew, D. P.; Handy, N. C. *Chem. Phys. Lett.* **2004**, *393*, 51–57; (b) Paterson, M. J.; Christiansen, O.; Pawłowski, F.; Jørgensen, P.; Hättig, C.; Helgaker, T.; Sałek, P. *J. Chem. Phys.* **2006**, *124*, 054322–054332; (c) Peach, M. J. G.; Helgaker, T.; Sałek, P.; Keal, W.; Lutns, O. B.; Tozer, D. J.; Handy, N. C. *Phys. Chem. Chem. Phys.* **2006**, *8*, 558–562.
9. Bruhn, T.; Hemberger, Y.; Schaumlöffel, A.; Bringmann, G. *SpecDis Version 1.53*; University of Wuerzburg: Wuerzburg, Germany, 2011.
10. Santoro, F.; Improta, R.; Lami, A.; Bloino, J.; Barone, V. *J. Chem. Phys.* **2008**, *128*, 224311–224328.
11. Lin, N.; Solheim, H.; Ruud, K.; Nooijen, M.; Santoro, F.; Zhao, X.; Kwit, M.; Skowronek, M. *Phys. Chem. Chem. Phys.* **2012**, *14*, 3669–3680.
12. Santoro, F. FCclasses a Fortran 77 code. See: http://village.pi.iccom.cnr.it [last accessed 10.07.13]; (b) Cerezo, F. "TDspectrum" a routine for TD calculations within FCclasses.
13. Avila Ferrer, F. J.; Santoro, F. *Phys. Chem. Chem. Phys.* **2012**, *14*, 13549–13563.
14. Santoro, F.; Barone, V. *Int. J. Quantum Chem.* **2010**, *110*, 624–636.
15. Tatchen, J.; Pollack, E. *J. Chem. Phys.* **2008**, *128*, 164303–164317.
16. Lightner, D. A.; Gurst, J. E. *Organic Conformational Analysis and Stereochemistry from Circular Dichroism Spectroscopy*; Wiley-VCH: New York, NY, 2000.
17. Djerassi, C.; Krakower, G. W. *J. Am. Chem. Soc.* **1959**, *81*, 94–101.
18. Lightner, D. A.; Docks, E. L. *Tetrahedron* **1979**, *35*, 713–720.
19. Mennucci, B.; Tomasi, J. *J. Phys. Chem. A* **2002**, *106*, 6102–6113.
20. He, J.; Petrovic, A. G.; Polavarapu, P. L. *J. Phys. Chem. B* **2004**, *108*, 20451–20457.
21. Devlin, F. J.; Stephens, P. J. *J. Am. Chem. Soc.* **1999**, *121*, 7413–7414.
22. (a) Holzwarth, G.; Hsu, E. C.; Mosher, H. S.; Faulkner, T. R.; Moscowitz, A. *J. Am. Chem. Soc.* **1974**, *96*, 251–252; (b) Nafie, L. A.; Cheng, J. C.; Stephens, P. J. *J. Am. Chem. Soc.* **1975**, *97*, 3842–3843; (c) Nafie, L. A.; Keiderling, T. A.; Stephens, P. J. *J. Am. Chem. Soc.* **1976**, *98*, 2715–2723.
23. (a) Longhi, G.; Abbate, S.; Gangemi, R.; Giorgio, E.; Rosini, C. *J. Phys. Chem. A* **2006**, *110*, 4958–4968; (b) Abbate, S.; Burgi, L. F.; Gangemi, F.; Gangemi, R.; Lebon, F.; Longhi, G.; Pultz, V. M.; Lightner, D. A. *J. Phys. Chem. A* **2009**, *113*, 11390–11405.
24. Laux, L.; Pultz, V. M.; Abbate, S.; Havel, H. A.; Overend, J.; Moscowitz, A.; Lightner, D. A. *J. Am. Chem. Soc.* **1982**, *104*, 4276–4278.
25. Gangemi, R.; Longhi, G.; Lebon, F.; Abbate, S.; Laux, L. *Monatsh. Chem.* **2005**, *136*, 325–345.
26. (a) Hayashi, T.; Yamazaki, K. *Chem. Rev.* **2003**, *103*, 2829–2844; (b) Iuliano, A. *Tetrahedron: Asymmetry* **2010**, *21*, 1943–1958.